International Journal of Medical Physics, Clinical Engineering and Radiation Oncology, 2019, 8, 46-56
http://www.scirp.org/journal/ijmpcero
ISSN Online: 2168-5444
ISSN Print: 2168-5436

Study of Image Contrast Recovery Coefficient (CRC) of a Large Ring PET Scanner

M. M. Ahasan[1], S. Akter[2], R. Khatun[2], M. F. Uddin[1], M. R. Islam[1], H. M. Jamil[1], A. N. Monika[1], M. A. Rahman[1], R. P. Das[1], M. M. Rahman[2], R. A. Sharmin[1], M. N. Khanam[3]

[1]Institute of Nuclear Medical Physics, AERE, Bangladesh Atomic Energy Commission, Dhaka, Bangladesh
[2]Atomic Energy Centre, Bangladesh Atomic Energy Commission, Dhaka, Bangladesh
[3]Infertility Unit, Department of Gynaecology & Obstetrics, Bangabandhu Sheikh Mujib Medical University, Dhaka, Bangladesh
Email: *monjur_ahasan@yahoo.co.uk

How to cite this paper: Ahasan, M.M., Akter, S., Khatun, R., Uddin, M.F., Islam, M.R., Jamil, H.M., Monika, A.N., Rahman, M.A., Das, R.P., Rahman, M.M., Sharmin, R.A. and Khanam, M.N. (2019) Study of Image Contrast Recovery Coefficient (CRC) of a Large Ring PET Scanner. *International Journal of Medical Physics, Clinical Engineering and Radiation Oncology*, **8**, 46-56.
https://doi.org/10.4236/ijmpcero.2019.81005

Received: December 27, 2018
Accepted: February 19, 2019
Published: February 22, 2019

Abstract

Image contrast recovery coefficient (CRC) of a large ring PET scanner "macroPET" was studied with septa and without septa configuration by acquiring data from a laboratory made 35.7 cm square phantom filled with 18-F. Images were reconstructed with simple 2D filtered back projection using Hann, Hamming and Parsen filters with different cut-off frequencies aiming to investigate the influence of filter and cut-off frequency on image contrast with septa and without septa mode. Results indicate that the CRC, for both hot and cold lesions, is excellent for diameters ≥ 3 cm using cut-off frequencies > 0.4. For a 2 cm hot lesion CRC is around 0.8 to 0.9. CRC for 1 cm hot and cold lesions is ~0.3, as expected. There is surprisingly little difference between results with and without septa. For hot lesions, septa appear to improve CRC slightly, but for cold lesions CRC is slightly poorer using septa.

Keywords

PET, Filter, Septa & CRC

1. Introduction

Positron emission tomography (PET) is a nuclear imaging technique which has been widely used over the last few decades in many clinical applications such as staging, evaluating treatment response, and predicting prognosis in malignant diseases [1] [2].

A large ring PET "macroPET" system was constructed as a prototype by reconfiguring components from an original ECAT 951 system [3]. The original system had 32 detector modules ("buckets" or "packs") mounted in two rings

with an inner diameter of 100 cm and a 10.8 cm axial FOV. But in the macroPET system [4], the 32 modules are mounted in a single ring with an inner diameter of 2.34 m. As in original system, the modified design has also 128 BGO blocks, 512 PMTs, 8192 individual detectors, 8 crystal rings and 1024 detectors per crystal ring. It was not practicable to construct dedicated septa [5] for macroPET, but in an attempt to investigate the value of septa some measurements were performed using the septa from the original ECAT 951 and the results compared with those obtained without any septa. Septa are lead or tungsten materials which are extended the scanner allow only data for direct and adjacent planes to be collected. Septa reduce most of the scatter events and also reduce photon flux from outside the field of view (FOV), but block many true events, and hence limit the scanner sensitivity.

Apart from these septa, macroPET has no shielding against out of field activity, which can give rise to high backgrounds of random and scattered events. Ultimately if a large ring scanner were to be used in real studies it would be necessary to add side shielding, but for the present trials these problems have been partly avoided by using phantoms. A large ring PET "macroPET" system was constructed as a prototype to demonstrate the feasibility of performing PET scans on a large scale. After design, setup and calibration of the macro PET system, initial results of its performance characteristics were experimentally studied [6] [7]. In this study, an effort has been made to investigate the influence of filter and cut-off frequency on image contrast with septa and without septa acquisition.

2. Methods

A 35.7 cm^2 square phantom with warm background embedded by 3 hot and 2 cold lesions (five small cylinders) was scanned in septa and no-septa mode for the contrast recovery (CR) study. The cylinders containing high activity (hot lesions) were 4, 2, and 1 cm diameter and all have the same uptake value in each acquisition mode. The diameters of cylinders containing inactive water (cold lesions) were 3 and 1 cm. The phantom used in the study was filled with F-18 radioisotope to a depth of about 5 cm to avoid any effect of out-of-field of activity. The concentration of F-18 radioactivity ratio of the hot lesions to the warm background was approximately 7.2:1 for no-septa and 8.5:1 for septa mode.

Images were reconstructed using Hann, Hamming and Parsen filters with different cut-off frequencies.

The Hann function, named after the Austrian meteorologist Julius von Hann, is a discrete window function given by

$$w(n) = 0.5\left[1 - \cos\left(\frac{2\pi n}{N-1}\right)\right] = \sin^2\left(\frac{\pi n}{N-1}\right)$$

and sometimes referred to as Hanning, presumably due to its linguistic and formulaic similarities to the Hamming window.

In each case, attenuation correction was performed using attenuation factors

for each measured LOR which had previously been calculated using the known geometry and an attenuation coefficient of 0.095 cm^{-1} for 511 keV gamma-rays in water. This attenuation correction is quite sensitive to the orientation assumed for the phantom. Trial and error was used to find the position and orientation of the phantom in the attenuation calculations which gave minimum artefacts in the reconstructed images.

The hot lesion contrast recovery coefficient (CRC_{hot}) is calculated as [8]:

$$CRC_{\text{hot}} = \frac{C_{\text{hot}} - C_{\text{warm}}}{C_{\text{warm}}} \div \frac{a_{\text{hot}} - a_{\text{warm}}}{a_{\text{warm}}} \tag{1}$$

where C_{hot} and C_{warm} are the average of the counts measured using the PET system in the hot sphere ROI and the average of the counts in all warm ROIs respectively. a_{hot} and a_{warm} are the activities in the hot and warm background regions respectively. The cold sphere CRC (CRC_{cold}) is calculated as:

$$CRC_{\text{cold}} = \frac{C_{\text{warm}} - C_{\text{cold}}}{C_{\text{warm}}} \tag{2}$$

where C_{cold} is the average of the counts measured in the cold sphere ROI. Counts were taken from the same place by drawing a 1 cm diameter ROI on the reconstructed PET image for each lesion.

3. Results

Figure 1 shows the image slice for the square phantom generated with two acquisition times. The images were reconstructed by a Hamming filter with cut-off frequency of 0.4. In the two counting statistics, three hot and two cold lesions are visible in each case. Image slice with 100 M events are more clearly visible than the slice with 50 M events as the more counts reduce the image noise, and hence improves the image appearance.

The square phantom images reconstructed using Hann, Hamming and Parsen filters and cut-off frequencies of 0.4 and 0.8 are shown in Figure 2. The images reconstructed by acquiring approximately 100 M coincidence events (13.3%

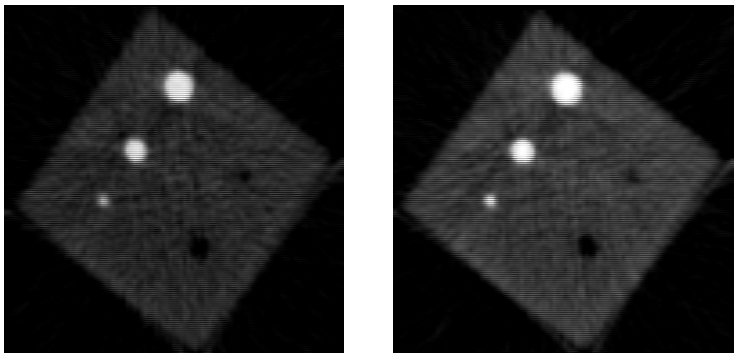

(a) (b)

Figure 1. Central slice for the 35.7 cm square image quality phantom generated two acquisition times in no-septa mode. (a) 50 M counts (20.74% randoms); (b) 100 M counts (13.3% randoms).

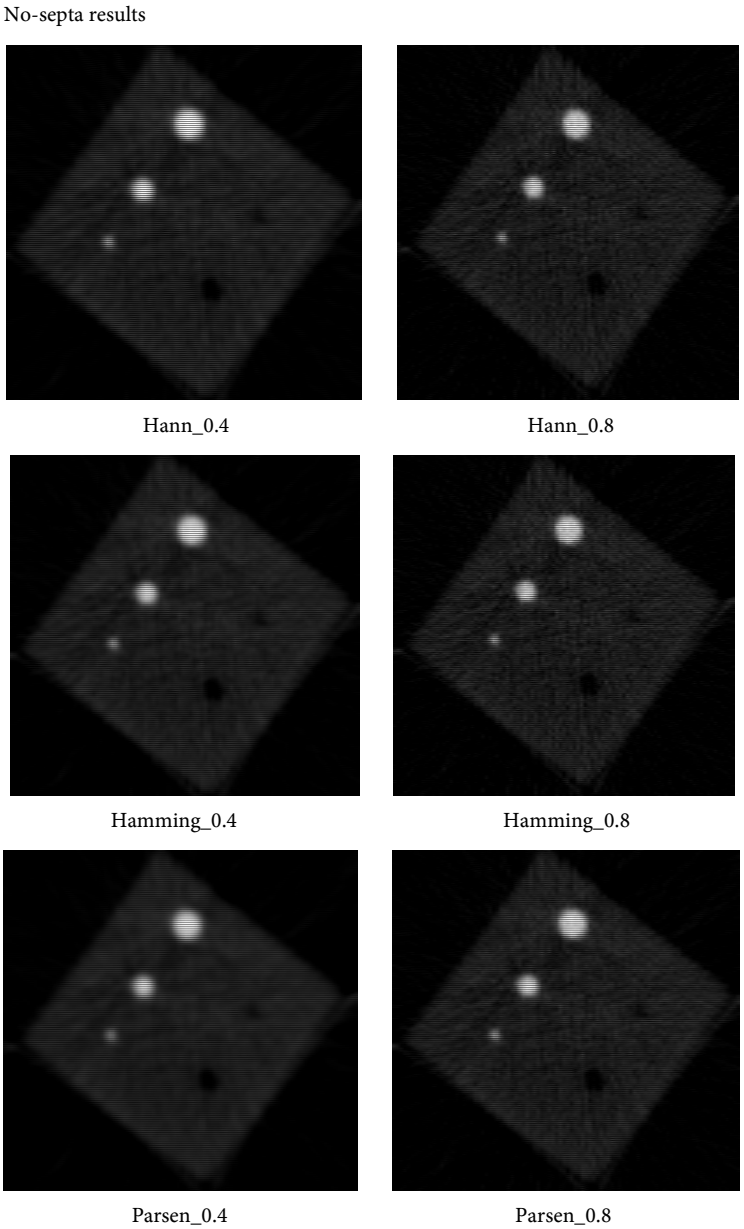

Figure 2. The images (slice 6) reconstructed with three filters (Hann, Hamming and Parsen) and its cut-off frequencies of 0.4 and 0.8 (no-septa mode).

randoms) in no-septa configuration. Three hot and two cold lesions are observable in all filter cases. There is no significant difference between the images generated from three filters in case of lesion detection as expected. In our previous study [9], it was very hard to make conclusion to choose the better filter from the reconstructed images. But the image generated by the Hamming filter with cut-off frequency of 0.4 and 0.8 may be slightly better visible than the other images.

Figure 3 shows the with-septa images generated using three filters (Hann, Hamming and Parsen) and its cut-off frequencies of 0.4 and 0.8. The images reconstruction performed by acquiring approximately 169 M events (12% randoms)

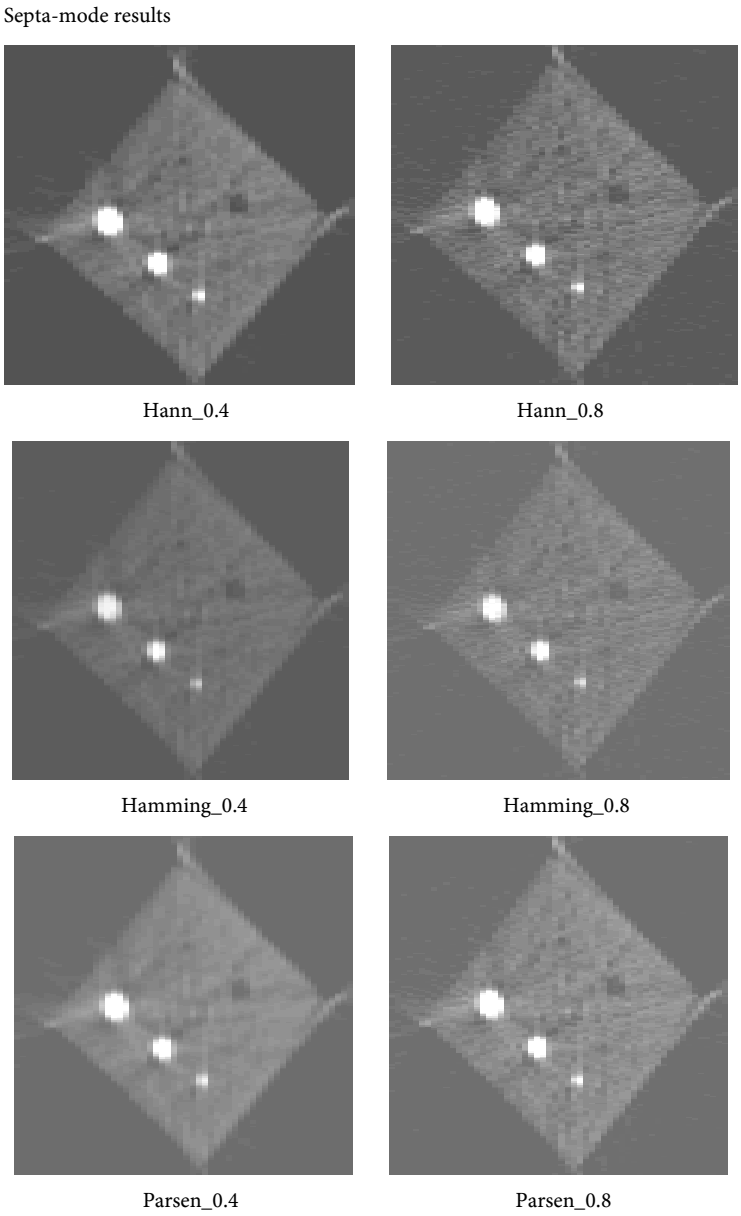

Figure 3. The images (slice 6) reconstructed with three filters (Hann, Hamming and Parsen) and its cut-off frequencies of 0.4 and 0.8 (septa mode).

with septa mode. Lesions (3 hot and 2 cold) are visible in case of Hamming and Parsen filter. The 1 cm cold lesion is very difficult to detect but 1 cm hot lesion is very clearly visible in all cases. No significant changes are observable among the images generated by different filters.

The contrast recovery coefficient (CRC) as a function of the cut-off frequency for the 4 cm hot lesion with no-septa is shown in **Figure 4**. **Figure 5** shows the corresponding results for the configuration with septa. The CRC results for all filter cases (Hamming, Hann and Parsen) are very similar, and the values are close to unity (slightly higher for the with septa mode) above a cut-off frequency of 0.4. The CRC curve is almost flat from cut-off frequency of 0.4 to 1.0 for both

modes. For the large lesion, there is a slight loss (around 10%) in CRC at cut-off frequency 0.2.

Figure 6 shows the CRC as a function of the cut-off frequency for the 2 cm hot lesion with no-septa and Figure 7 for the septa configuration. The CRC values are similar for both Hamming and Hann filters but slightly lower using the Parsen filter for both modes. Without septa, the values are approximately 0.85 above a cut-off frequency of 0.4. Adding septa improves these values by approximately 5% - 12%. There is a significant reduction in contrast recovery coefficient at a cut-off frequency of 0.2.

The CRC as a function of the cut-off frequency for the 1 cm hot lesion with no-septa is shown in Figure 8 and for the with septa configuration is shown in Figure 9. Again, both the Hamming and Hann filters give very similar results but the Parsen filter gives a lower CRC in both modes. The CRC for this small lesion is around 0.3, and addition of septa does not appreciably improve the contrast at cut-off frequencies above 0.6.

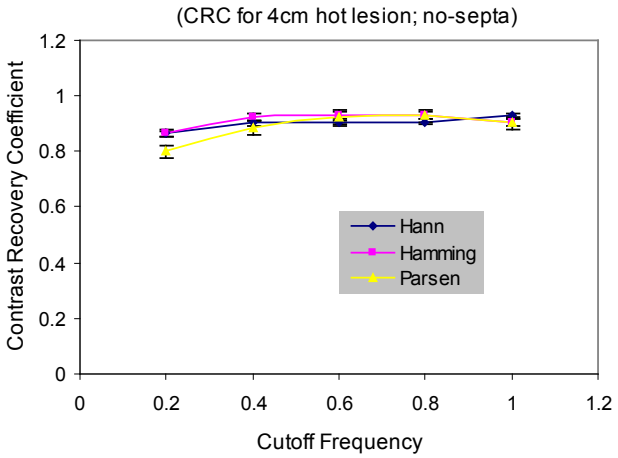

Figure 4. Contrast recovery coefficient for 4 cm hot lesion as a function of cut-off frequency for three filters with no-septa mode (slice 4).

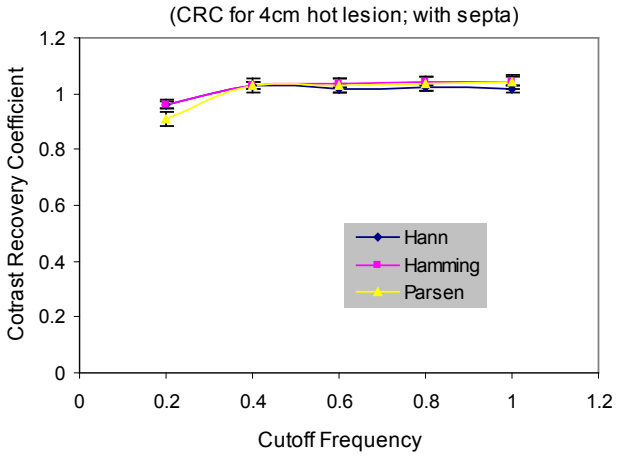

Figure 5. Contrast recovery coefficient for 4 cm hot lesion as a function of cut-off frequency for three filters with septa mode (slice 4).

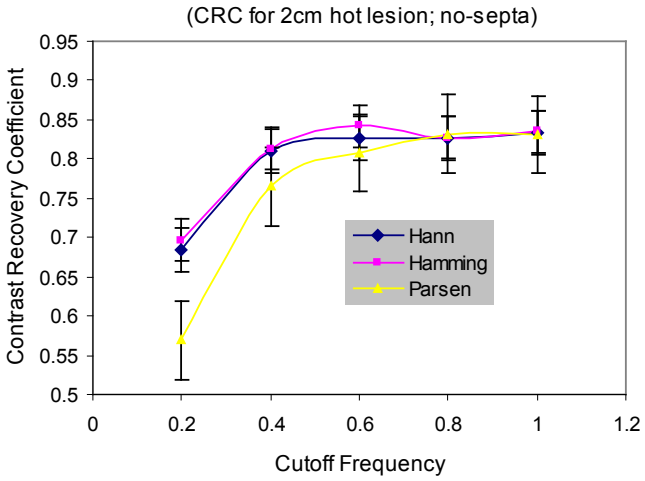

Figure 6. Contrast recovery coefficient for 2 cm hot lesion as a function of cut-off frequency for three filters with no-septa mode (slice 4).

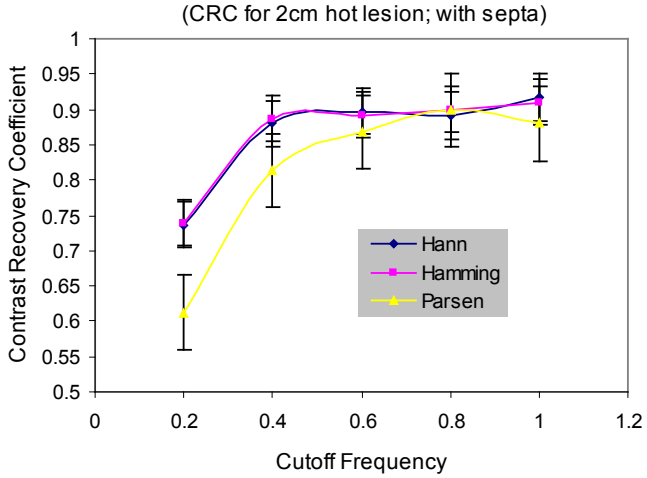

Figure 7. Contrast recovery coefficient for 2 cm hot lesion as a function of cut-off frequency for three filters with septa mode (slice 4).

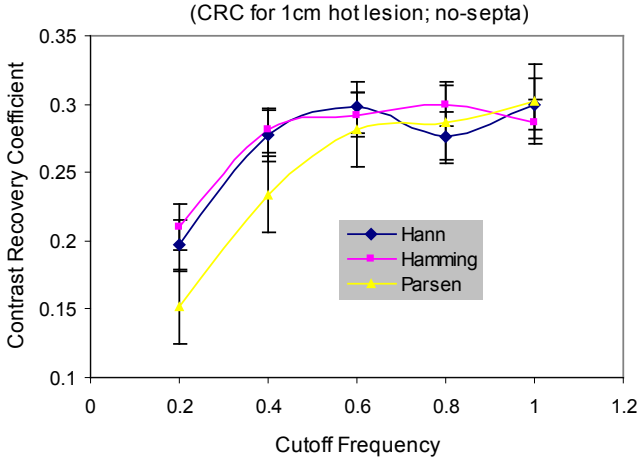

Figure 8. Contrast recovery coefficient for 1 cm hot lesion as a function of cut-off frequency for three filters with no-septa mode (slice 4).

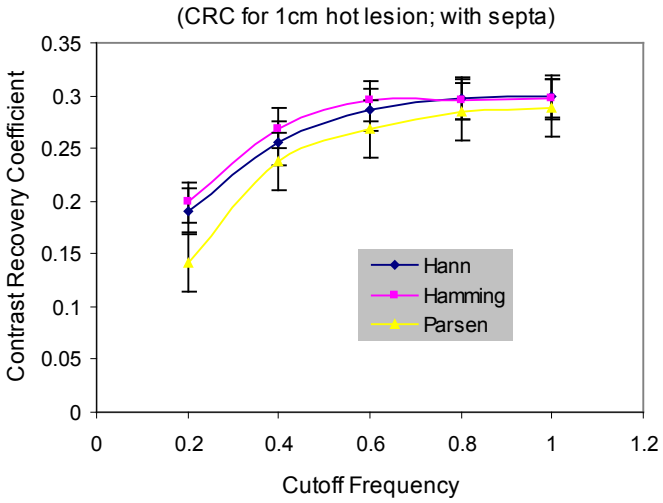

Figure 9. Contrast recovery coefficient for 1 cm hot lesion as a function of cut-off frequency for three filters with septa mode (slice 4).

4. Discussions

For the large (4 cm) lesion good values of CRC are obtained for most values of cut-off frequency, and addition of septa improves the CRC by around 10%, showing that the presence of scatter background is affecting these values. For the small (1 cm) lesion, contrast is limited by the spatial resolution of the scanner, and addition of septa has little effect. For the intermediate (2 cm) lesion, the results depend both on cut-off frequency and on the presence of septa. A general comparison of CRC results for this lesion is shown in **Figure 10**. The average of the CRC results for cut-off frequencies 0.4 to 1.0 is 0.83 without septa and 0.90 with septa, so that the septa increase the contrast by approximately 8% for this lesion.

The CRC for cold lesions as a function of cut-off frequency for Hamming window function in both acquisition modes is shown **Figure 11**. For the 3 cm cold lesion, good values of CRC are obtained for all cut-off frequencies above 0.4, and addition of septa appears to make little difference. For the 1 cm cold lesion, CRC results of up to 0.4 are obtained without septa, but addition of septa significantly worsens the CRC. The reason for this is not understood.

Figure 12 shows a horizontal profile running through the middle of the three hot lesions of the image plane 4 reconstructed by Hamming and Parsen filter with cut-off frequencies of 0.4 and 0.8. The peaks for three hot lesions (4 cm, 2 cm and 1 cm) are clearly distinguishable in the profile. The peak to warm background ratio for Hamming filter is slightly higher for 2 cm and 1 cm hot lesions than Parsen filter, and the profile result is consistent with **Figures 4-9** and also with **Figure 13** for profile running along the two cold lesions.

In the contrast phantom, CRC values close to unity can be achieved for the 2 cm and 4 cm hot lesions and for the 3 cm cold lesion (**Figure 4**). In For both the 1 cm hot and cold lesions the CRC is around 0.3. Contrast recovery is reduced when filter cut-off frequencies less than 0.4 are used. There is surprisingly little

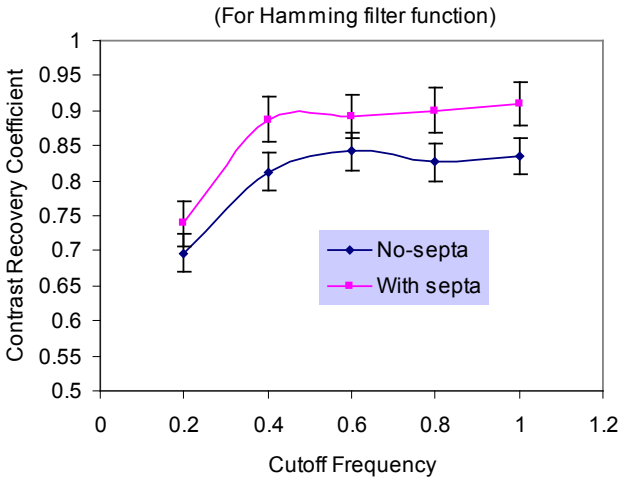

Figure 10. Comparison of CRC for the 2 cm hot lesion as a function of cut-off frequency for Hamming filters in septa and no-septa configurations (slice 4).

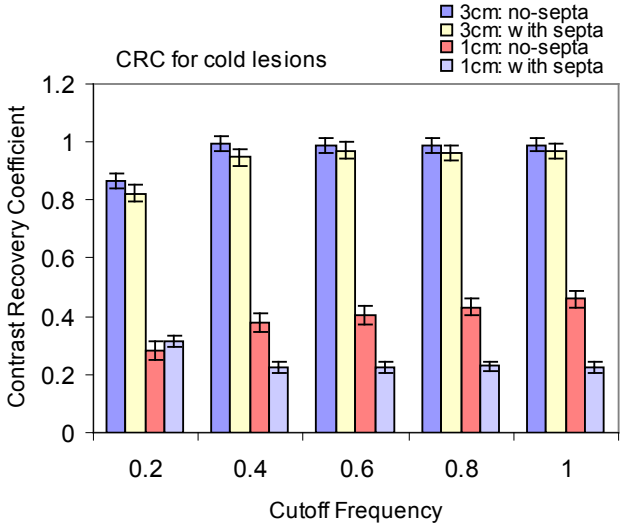

Figure 11. CRC for cold lesions as a function of cut-off frequency for Hamming window function in both acquisition modes (using slice 4).

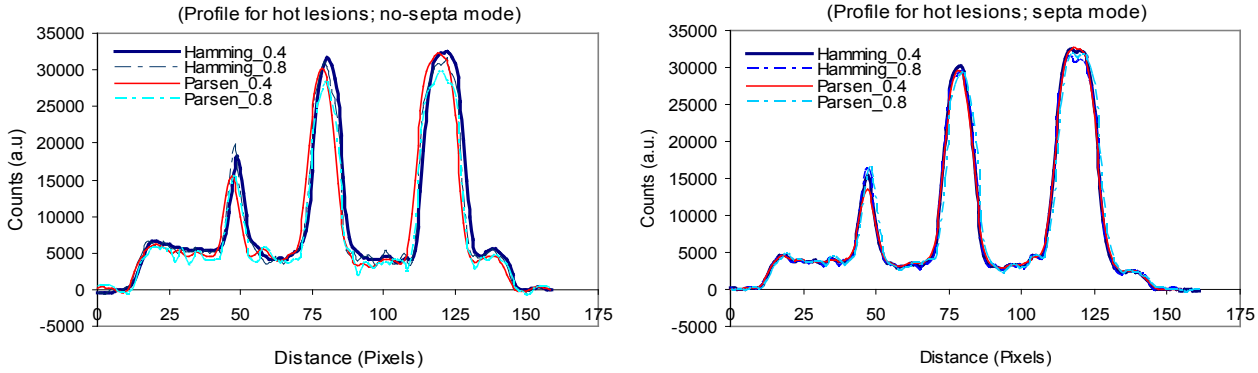

Figure 12. Horizontal profile running along the middle of three hot lesions (4 cm, 2 cm and 1 cm) of slice 4 reconstructed by Hamming and Parsen filter with cut-off frequencies of 0.4 and 0.8: (a) no-septa mode; (b) septa mode.

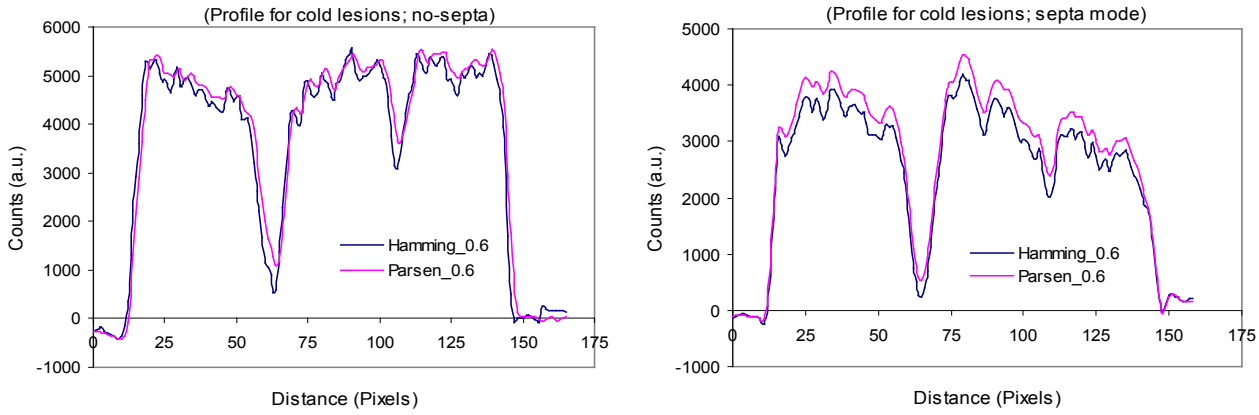

Figure 13. Horizontal profiles running along the middle of two cold lesions (3 cm and 1 cm): (a) in the image slice 4 (no-septa mode); (b) slice 10 (septa mode) reconstructed by Hamming and Parsen filter with cut-off frequency of 0.6.

difference between the results obtained with and without septa. For hot lesions, septa apparently improve CRC slightly, but for cold lesions CRC is slightly poorer using septa.

5. Conclusion

Using cut-off frequencies > 0.4, contrast recovery for both hot and cold lesions is excellent for diameters ≥ 3 cm. For a 2 cm hot lesion CRC is around 0.8 to 0.9. CRC for 1 cm hot and cold lesions is ~0.3, as expected. Using cut-off frequencies < 0.4 reduces contrast. There is surprisingly little difference between results with and without septa. For hot lesions, septa appear to improve CRC slightly, but for cold lesions CRC is slightly poorer using septa. Overall, the scanner performs as expected, taking account of its lower sensitivity and slightly poorer spatial resolution as compared to a clinical scanner. The main limitation in the study was the lack of shielding against out-of-field activity. In most cases measurements were performed with little out-of-field activity. The presence of such activity would add significantly to the background of random and scattered events. The septa used have only a limited effect in blocking out-of-field activity.

Conflicts of Interest

The authors declare no conflicts of interest regarding the publication of this paper.

References

[1] Kenjiro, A., Takayuki, K., Yoshifumi, S., Sachiko, K., Hideo, S., Norio, M. and Morihito, O. (2015) Utility of ^{18}F FDG-PET/CT for Predicting Prognosis of Luminal-Type Breast Cancer. *Breast Cancer Research and Treatment*, **150**, 209-217. https://doi.org/10.1007/s10549-015-3303-9

[2] Couto, P.J. and Milis, R.M. (2015) PET Imaging of Epigenetic Influences on Alzheimer's Disease. *International Journal of Alzheimer's Disease*, **2015**, Article ID: 575078. https://doi.org/10.1155/2015/575078

[3] Testing & Diagnostics (1985) Siemens Medical System. Service Manual. ECAT 951, 953.

[4] Ahasan, M.M. and Parker, D.J. (2008) Initial Results from a Prototype Large (2 m) Ring PET Scanner. In: Gelman, L., Hukins, D.W., Hunter, A. and Korsunsky, A.M., Eds., *Proceedings of the World Congress on Engineering* 2008, Lecture Notes in Engineering and Computer Science, London, 2-4 July 2008, Vol. 1, 676-681.

[5] Madsen, T.M., Anderson, A.J., Halama, R.J., Kleck, J., Simpkin, J.D., Votaw, R.J., Williams, E.L., William, E.L. and Yester, V.M. (2006) AAPM Task Group 108: PET and PET/CT Shielding. *Medical Physics*, **339**, 4-15. https://doi.org/10.1118/1.2135911

[6] Ahasan, M.M. and Parker, D.J. (2009) Design and Initial Performance Evaluation of a Prototype Large Ring PET Scanner. In: Ao, S.I., *et al*., Eds., *Advances in Electrical Engineering and Computational Science*, Springer, New York City, Vol. 14, 161-172.

[7] Ahasan, M.M. and Parker, D.J. (2009) Design and Coincidence Issues of a Small Ring PET Camera. *Bangladesh Journal of Nuclear Medicine*, **12**, 138-141.

[8] Daube-Witherspoon, M.E., Karp, J.S., Casey, M.E., DiFilippo, F.P., Hines, H., Muehllehner, G., Simcic, V., Stearns, C.W., Adam, L.E., Kohlmyer, S. and Sossi, V. (2002) PET Performance Measurements Using the NEMA NU 2-2001 Standard. *Journal of Nuclear Medicine*, **43**, 1398-1409.

[9] Ahasan, M.M., Akter, S., Khatun, R., Uddin, M.F., Monika, A.N., Rahman, M.A. and Khanan, M.N. (2017) Image Noise Analysis of a Large Ring PET Scanner. *International Journal of Medical Physics, Clinical Engineering and Radiation Oncology*, **6**, 208-215. https://doi.org/10.4236/ijmpcero.2017.62019